Int. J. Solids Structures Vol. 29, No. 23, pp. 2829-2854, 1992
Printed in Great Britain.

0020-7683/92 $5.00+.00

STRESS PROFILES AROUND A FIBER BREAK IN A COMPOSITE WITH A NONLINEAR, POWER LAW CREEPING MATRIX

DEBORAH D. MASON,† CHUNG-YUEN HUI and S. LEIGH PHOENIX
Department of Theoretical and Applied Mechanics, Kimball Hall, Cornell University, Ithaca, NY 14853, U.S.A.

(*Received* 18 *January* 1992; *in revised form* 23 *April* 1992)

Abstract—A model is developed for the time evolution of the stresses and displacements around a fiber break in a simple planar composite loaded in tension. The composite consists of parallel, elastic fibers in a matrix that creeps according to a nonlinear, power law with memory, and which has exponents for both time and shear stress. Cases of three- and five-fiber composites are analysed using a shear-lag approximation which yields self-similar, closed-form solutions for fiber stresses, strains and displacements and for matrix shear stresses near the break. The exponents for the self-similar growth of the deformation zone, in both time and composite stress, are different from those of the matrix constitutive law. The length of the deformation zone is found typically to be finite at any given time in contrast to the case where the matrix is assumed to be linearly viscoelastic. Asymptotic results are obtained for the case of a high creep exponent in stress. These asymptotic results are similar to those for a perfectly plastic matrix material.

1. INTRODUCTION

In recent statistical models for the creep rupture of graphite fiber/epoxy composites, time dependent matrix deformation and interface debonding have been implicated as key mechanisms in the failure process (Phoenix *et al.*, 1988; Otani *et al.*, 1991). An early model of micromechanical creep processes actually dates back to Lifshitz and Rotem (1970). Failure in such unidirectional composites is generally a complex statistical process beginning with the random failure of fibers at flaw sites, followed by overloading of neighboring fibers by way of stress transfer through the matrix. Additional fibers fail leading to the growth of clusters of breaks and instability. In creep rupture, failure is also driven by viscoelastic creep in the polymer matrix near fiber breaks, which produces a widening overload profile on fibers next to existing breaks.

A shear-lag model for the time evolution of overstress profiles near broken fibers was developed recently by Lagoudas *et al.* (1989) under the assumption that the matrix is linearly viscoelastic and follows a power law, creep compliance in shear, a common assumption for polymers. Apart from the time dependence, their basic assumptions were those of the planar model of Hedgepeth (1961) with none of the complications introduced by considering normal stresses in the matrix or longitudinal yielding and splitting (Goree and Gross, 1979), or three-dimensional arrays (Hedgepeth and Van Dyke, 1967; Goree and Gross, 1980).

While the results of Lagoudas *et al.* (1989) provide valuable insight, the linearity of the matrix constitutive law in shear stress is not consistent with the deformation behavior of many polymeric matrices in the highly constrained, microscopic region between fibers near a break. Gulino *et al.* (1991) observed that a typical epoxy undergoes large-scale yielding and even slight strain softening up to strains of 30–40% before rapid strain hardening and failing, in contrast to the stress–strain behavior in bulk, which appears almost linear up to brittle failure at a strain of 2–4%. This large-scale yielding was studied extensively in thin films of a variety of epoxies by Glad (1986). Strain hardening was the result of crosslinking in the polymer network and can be delayed if the crosslink density is reduced. If a power law in stress is fitted to such a stress–strain behavior up to the point of strain hardening, one requires an exponent of 4–10 to achieve a reasonable fit.

†Present address: Polaroid Corporation, 565 Technology Square, Cambridge, MA 02139, U.S.A.

On the other hand, the authors are aware of no experimental studies of polymer creep in such microscopic regions at these high shear stress levels. Nevertheless, one might anticipate that a power law in time would still provide a useful model, though with exponents that might be larger than in the linear region. Thus we propose a nonlinear creep law, which is a power law in both stress and time and which has a memory integral to accommodate time variation and shear stresses in the polymer matrix. The model ignores the elastic component of matrix deformation so that the results apply only for large deformations or long times beyond the transient region. We give no justification for the model in terms of molecular kinetics except that power-law forms have been justified by Phoenix and Tierney (1983) in the case of the breakdown of fibers by chain scission, and a chain slippage version for creep is plausible.

In the present work, we consider the shear-lag model used by Lagoudas *et al.* (1989) but with a different constitutive law for the creep of the matrix as outlined above. We consider planar composites involving three and five fibers of infinite length. In Section 2 we describe the model in the case of three fibers. The middle fiber is assumed to be broken at time zero and we give governing equations for determining the evolution of the stresses, strains and displacements in the fiber as well as the matrix shear stresses. In Section 3 we consider the special case where the exponent in time is unity. This restriction allows us to obtain a solution in closed form. In Section 4 we present the numerical solution of the general case where the exponent in time in the power law model is arbitrary. In Section 5 we extend the analysis to a composite with five fibers. Section 6 provides some conclusions on the implications of the results.

2. DESCRIPTION OF THE MODEL WITH THREE FIBERS

Consider a planar arrangement of three fibers in a matrix as shown in Fig. 1, which shows only the right half since the problem is symmetric about the vertical axis. The fibers are parallel, infinitely long, equally spaced and linearly elastic. They are embedded in a matrix material which is nonlinear and creeps according to

$$\frac{\partial \gamma(x,t)}{\partial t} = B\tau(x,t)^m n\left[\int_0^t \tau(x,s)^m \,\mathrm{d}s\right]^{n-1}, \tag{1}$$

where $\gamma(x,t)$ is the matrix shear strain, $\tau(x,t)$ is the matrix shear stress (assumed not to change sign with time at fixed x) and B, m and n are positive material constants. (The parameters m and n are dimensionless and B has dimensions of stress^{-mn} · time^{-n}.) We restrict our attention to the ranges $0 < n \leqslant 1$ and $m > 1$, which are believed to be those of

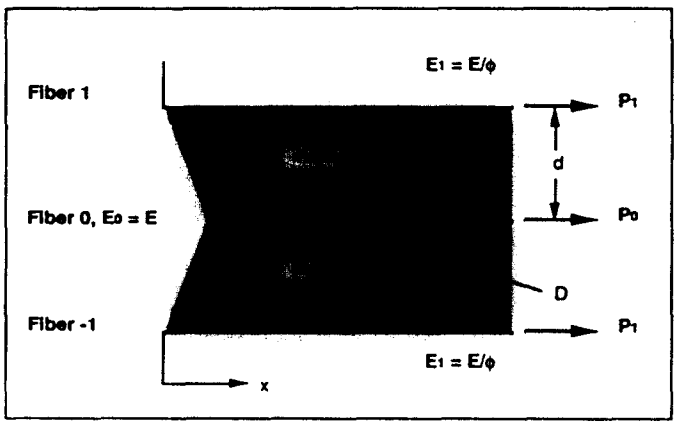

Fig. 1. Physical configuration for the three-fiber problem. The center fiber is broken at $x = 0$, $t = 0$. Only the right half is shown.

practical interest. When subjected to constant shear stress τ, a material of this form exhibits a shear strain rate of

$$\frac{\partial \gamma}{\partial t} = B\tau^{mn} n t^{n-1}, \tag{2}$$

or, shear strain as a function of time given by

$$\gamma = B\tau^{mn} t^{n}. \tag{3}$$

Thus the basic power law exponents for creep are n (time) and mn (shear stress). The matrix is assumed to have negligible tensile stiffness relative to that of the fibers, and thus offers no resistance to extensional deformations.

The fibers, denoted 1, 0 and -1 are of diameter D, cross-sectional area A, and inter-fiber spacing d. Thus the matrix on either side is taken to have width d, and thickness D. The Young's modulus of Fiber 0 is $E_0 = E$, while that of Fibers 1 and -1 is $E_1 = E_{-1} = E/\phi$, where ϕ is a parameter satisfying $0 \leqslant \phi \leqslant 1$ and is used to simulate different boundary conditions. For example, when $\phi = 0$, $E_1 \to \infty$, Fibers 1 and -1 are infinitely stiff, so that they appear essentially as rigid walls to the center fiber and the attached matrix. We refer to this as the single fiber problem. When $\phi = 1$, the fibers are of equal stiffness, whereas when $\phi = 0.5$, Fiber 0 is half as stiff as each outside fiber.

Loads are applied as follows: the respective fiber loads, P_0 and $P_1 = P_{-1}$ are applied at $x = \pm\infty$, such that they initially generate a uniform strain $\varepsilon = P_0/(AE) = P_1/(AE_1)$ in the material. The center fiber is suddenly broken at $x = 0$, $t = 0$. The force lost by the broken fiber is transferred, through shear tractions in the matrix, to the two intact neighbors. Due to the obvious symmetry, the displacements, strains and forces will be identical in Fibers 1 and -1. Thus, it is sufficient to restrict our attention to Fibers 0 and 1 throughout the discussion.

Free body diagrams for segments of Fibers 0 and 1 are shown in Fig. 2. Using Hooke's law, the force equilibrium equation for Fiber 0 is

$$2D\tau(x, t) = EA\frac{\partial^2 v_0(x, t)}{\partial x^2}, \tag{4}$$

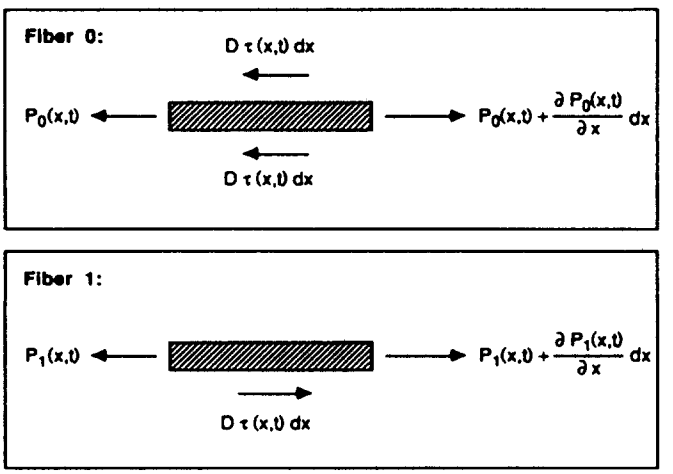

Fig. 2. Free body diagrams of segments of Fibers 0 and 1.

and for Fiber 1 is

$$-D\tau(x,t) = \frac{EA}{\phi}\frac{\partial^2 v_1(x,t)}{\partial x^2}, \tag{5}$$

where $v_i(x,t)$ is the displacement in Fiber i, for $i = 0, 1$ and τ is assumed to be constant across the thickness of the matrix. The initial and boundary conditions for Fiber 0 are

$$\begin{aligned} v_0(x>0, t=0) &= \varepsilon x = \frac{P_0}{AE}x, \\ v_{0,x}(x\to\infty, t\geqslant 0) &= \varepsilon, \\ v_{0,x}(x=0, t>0) &= 0, \end{aligned} \tag{6}$$

and for Fiber 1 are,

$$\begin{aligned} v_1(x>0, t=0) &= \varepsilon x, \\ v_{1,x}(x\to\infty, t\geqslant 0) &= \varepsilon, \\ v_{1,x}(x=0, t>0) &= \frac{P_0+2P_1}{2A(E/\phi)} = \varepsilon\left[1+\frac{\phi}{2}\right]. \end{aligned} \tag{7}$$

Since the relation between stresses and fiber displacements, eqns (4) and (5), are insensitive to the addition of a uniform strain ε, a compression model is devised with displacements, $u_i(x,t)$, defined as

$$u_i(x,t) = v_i(x,t) - \varepsilon x, \quad \text{for} \quad i = 0, 1 \text{ and } -1. \tag{8}$$

Fiber 0 is taken as already broken at $x = 0$, and a compressive force $P = AE\varepsilon$ is suddenly applied at $t = 0$ to the broken ends of Fiber 0, leading to strain $-\varepsilon$ at that point for all $t > 0$. From eqn (8), the solution for the tension problem can be recovered easily from the solution to the compression version by the addition of εx to the fiber displacements, and ε to the fiber strains. The shear stresses for both problems are identical.

In the compression version, the boundary and initial conditions are

$$\begin{aligned} u_0(x>0, t=0) &= 0, \\ u_{0,x}(x\to\infty, t\geqslant 0) &= 0, \\ u_{0,x}(x=0, t>0) &= -\varepsilon, \end{aligned} \tag{9}$$

for Fiber 0, and

$$\begin{aligned} u_1(x>0, t=0) &= 0, \\ u_{1,x}(x\to\infty, t\geqslant 0) &= 0, \\ u_{1,x}(x=0, t>0) &= \frac{\varepsilon\phi}{2}, \end{aligned} \tag{10}$$

for Fiber 1. Define

$$U(x,t) = u_0(x,t) - u_1(x,t). \tag{11}$$

In terms of $U(x, t)$ we have

$$\frac{\partial \gamma(x, t)}{\partial t} = \frac{1}{d} \frac{\partial U(x, t)}{\partial t} \tag{12}$$

for the shear strain rate in the matrix. From eqns (4), (5), (8) and (11) we obtain

$$\tau(x, t) = \frac{EA}{(2+\phi)D} \frac{\partial^2 U(x, t)}{\partial x^2}. \tag{13}$$

Combining eqns (1), (12) and (13), we obtain a single equation governing U, i.e.

$$\frac{\partial U}{\partial t} = dBn\left[\frac{EA}{(2+\phi)D}\right]^{mn} (U_{xx})^m \left[\int_0^t (U_{xx})^m \, ds\right]^{n-1}, \tag{14}$$

with the initial and boundary conditions:

$$\begin{aligned} U(x > 0, t = 0) &= 0, \\ U_x(x \to \infty, t \geqslant 0) &= 0, \\ U_x(x = 0, t > 0) &= -\varepsilon\left[1 + \frac{\phi}{2}\right]. \end{aligned} \tag{15}$$

Note that the matrix in each bay between two fibers couples the displacements in those bounding fibers.

3. ANALYTIC RESULTS FOR THE THREE-FIBER PROBLEM

Self-similar transformation

Dimensional considerations in terms of dimensionless groups imply that the solution for the fiber displacements has the form

$$U(x, t)/x\varepsilon(1 + \phi/2) = g(\eta), \tag{16}$$

where g is a function of the dimensionless parameter

$$\eta = \frac{x}{\varepsilon^{\alpha/\beta}(1+\phi/2)^{\alpha/\beta} Q_3^{\alpha} t^{\alpha}}, \tag{17}$$

where α and β are the dimensionless exponents

$$\alpha = \frac{n}{mn+1} \quad \text{and} \quad \beta = \frac{n}{mn-1} \tag{18}$$

and

$$Q_3 = (dB)^{1/n}\left[\frac{EA}{(2+\phi)D}\right]^m \tag{19}$$

having dimensions that render η dimensionless.

Consider first the special case of $n = 1$ where the matrix constitutive law, eqn (1), becomes memoryless. Substituting eqn (16) into eqn (14) gives

$$-\alpha\eta^2 g'(\eta) = [2g'(\eta) + \eta g''(\eta)]^m. \tag{20}$$

Equation (20) can be solved in closed form (Mason, 1990), giving

$$g'(\eta) = -\eta^{-2}[C - M\eta^2]^{m\beta}, \tag{21}$$

where C is an integration constant and

$$M = \frac{1}{2m\beta}\alpha^{1/m} = \frac{m-1}{2m}\left[\frac{1}{m+1}\right]^{1/m}. \tag{22}$$

Note that for $m > 1$, $M > 0$ so that for $\eta^2 > C/M$, $g'(\eta)$ is complex so that no real solution exists unless there exists a constant η_{max} such that for all $\eta > \eta_{max}$, $g'(\eta) = 0$. This implies the existence of a right moving boundary point beyond which all displacements and stresses would be identically zero. Indeed, if we define η_{max} as

$$\eta_{max} = \left[\frac{C}{M}\right]^{1/2}, \tag{23}$$

then $g'(\eta_{max}) = 0$. If we further require $g(\eta_{max}) = 0$, then it can be verified that the boundary conditions of eqn (15) and the governing eqn (14), can be satisfied if we require $g(\eta) = 0$ for all $\eta > \eta_{max}$. These boundary conditions are replaced by:

$$g(\eta = \eta_{max}) = 0,$$
$$g'(\eta = \eta_{max}) = 0, \tag{24}$$

so that

$$g(\eta) = -\int_{\eta}^{\eta_{max}} g'(z)\,dz = \int_{\eta}^{\eta_{max}} z^{-2}[C - Mz^2]^{m\beta}\,dz. \tag{25}$$

Substituting eqn (25) into eqn (16), the initial condition $U_x(x = 0, t > 0) = -\varepsilon(1 + \phi/2)$ in eqn (15) is found, after some manipulations, to be equivalent to

$$2m\beta\sqrt{M}C^{\beta+1/2}\left\{\int_0^1 (1-\omega^2)^{\beta}\,d\omega\right\} = 1, \tag{26}$$

which implies that

$$\eta_{max} = \frac{1}{\sqrt{M}}\left[\frac{1}{m\beta\sqrt{M\pi}}\,\frac{\Gamma\{\beta+3/2\}}{\Gamma\{\beta+1\}}\right]^{2/\beta}, \tag{27}$$

where Γ is the Gamma function and we have used the idéntity

$$\int_0^1 (1-\omega^2)^{\beta}\,d\omega = \frac{1}{2}\left[\frac{\Gamma\{1/2\}\Gamma\{\beta+1\}}{\Gamma\{\beta+3/2\}}\right].$$

From eqns (27) and (22) it is evident that $\eta_{max} \to 1$ as $m \to \infty$, and $\eta_{max} \to \infty$ as $m \to 1$ where the material becomes linearly viscous. Let x_{max} be the physical length of the loaded zone corresponding to the value $\eta = \eta_{max}$. From eqns (18) and (27), and incorporating the definitions of α, β and Q_3 we obtain

$$x_{\max} = \varepsilon^{(m-1)/(m+1)}(1+\phi/2)^{-1/(m+1)} t^{1/(m+1)} \left[\frac{EA}{D}\right]^{m/(m+1)} \left[dB\frac{m(m+1)}{m-1}\right]^{1/(m+1)} \cdot \left[\frac{\Gamma\left\{\frac{3m-1}{2m-2}\right\}}{\sqrt{\pi}\Gamma\left\{\frac{m}{m-1}\right\}}\right]^{(m-1)/(m+1)}. \quad (28)$$

Equation (28) implies that, for sufficiently large m, the region where stresses and strains are nonzero spreads out approximately proportionally to the applied strain and is very insensitive to time.

The shear stress, $\tau(x, t)$, in the matrix is found to be

$$\tau(x,t) = \frac{AE\varepsilon}{D\sqrt{\pi}} \frac{\Gamma\{\beta+3/2\}}{\Gamma\{\beta+1\}} \frac{1}{x_{\max}} \left[1-\left[\frac{\eta}{\eta_{\max}}\right]^2\right]^{\beta}. \quad (29)$$

For convenience we define a nondimensional shear stress $\hat{\tau}(y)$, where $y = \eta/\eta_{\max}$, as

$$\hat{\tau}(y) = \frac{\tau(x,t)2Dx_{\max}}{AE\varepsilon} = \frac{2}{\sqrt{\pi}} \frac{\Gamma\{\beta+3/2\}}{\Gamma\{\beta+1\}} [1-y^2]^{\beta}. \quad (30)$$

Figure 3 is a plot of $\hat{\tau}(y)$ versus y for several values of m. As $m \to \infty$, $\hat{\tau}(y) \to 1$, for $0 \leqslant y \leqslant 1$ (corresponding to $0 \leqslant \eta \leqslant \eta_{\max}$), and is zero elsewhere.

The strains can be computed using eqn (11), i.e.

$$U_x(x,t) = u_{0,x}(x,t) - u_{1,x}(x,t) = \varepsilon_0(x,t) - \varepsilon_1(x,t), \quad (31)$$

where $\varepsilon_i(x, t)$ for $i = 0, 1$, are the individual fiber strains. The strains are also related through global force equilibrium of the composite so that

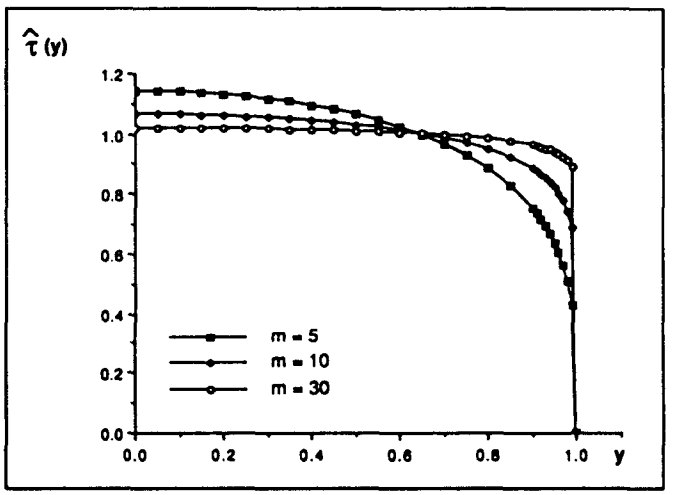

Fig. 3. Plot of nondimensional shear stress profile $\hat{\tau}(y)$ versus scaled distance y for $n = 1$ and several values of m. Later in the text $\hat{\tau}(y)$ is $\eta_{\max} H''(y\eta_{\max})$.

$$\varepsilon_1(x,t) = -\frac{\phi}{2}\varepsilon_0(x,t). \tag{32}$$

Therefore,

$$U_r(x,t) = \left[1+\frac{\phi}{2}\right]\varepsilon_0(x,t)$$

$$= -\left[\frac{2}{\phi}+1\right]\varepsilon_1(x,t). \tag{33}$$

From eqns (16) and (25), we obtain

$$\varepsilon_0(x,t) = -\varepsilon\frac{2}{\sqrt{\pi}}\frac{\Gamma\{\beta+3/2\}}{\Gamma\{\beta+1\}}\int_{\eta/\eta_{\max}}^{1}(1-\omega^2)^{\beta}\,d\omega, \tag{34}$$

and

$$\varepsilon_1(x,t) = \varepsilon\frac{\phi}{2}\frac{2}{\sqrt{\pi}}\frac{\Gamma\{\beta+3/2\}}{\Gamma\{\beta+1\}}\int_{\eta/\eta_{\max}}^{1}(1-\omega^2)^{\beta}\,d\omega. \tag{35}$$

The fiber forces are related to the strains by

$$P_0(x,t) = AE\varepsilon_0(x,t) \tag{36}$$

and

$$P_1(x,t) = \frac{AE}{\phi}\varepsilon_1(x,t) = -\frac{AE}{2}\varepsilon_0(x,t). \tag{37}$$

It is useful to define nondimensional forms of the forces and strains. Let $y = \eta/\eta_{\max}$. In $0 \leqslant y \leqslant 1$, define a nondimensional fiber force, $\hat{P}(y)$, by

$$\hat{P}(y) = \frac{P_0(x,t)}{AE\varepsilon} = -\frac{2}{\sqrt{\pi}}\frac{\Gamma\{\beta+3/2\}}{\Gamma\{\beta+1\}}\int_{y}^{1}(1-\omega^2)^{\beta}\,d\omega, \tag{38}$$

which may also be viewed as a nondimensional strain, $\hat{\varepsilon}(y)$. From eqns (36) to (37) we have

$$P_0(x,t) = AE\varepsilon\hat{P}(y), \tag{39}$$

and

$$P_1(x,t) = -\frac{AE\varepsilon}{2}\hat{P}(y). \tag{40}$$

The fiber strains may also be written in terms of the nondimensional force, $\hat{P}(y)$. From eqns (34), (35) and (38),

$$\varepsilon_0(x,t) = \varepsilon\hat{\varepsilon}(y) = \varepsilon\hat{P}(y) \tag{41}$$

and

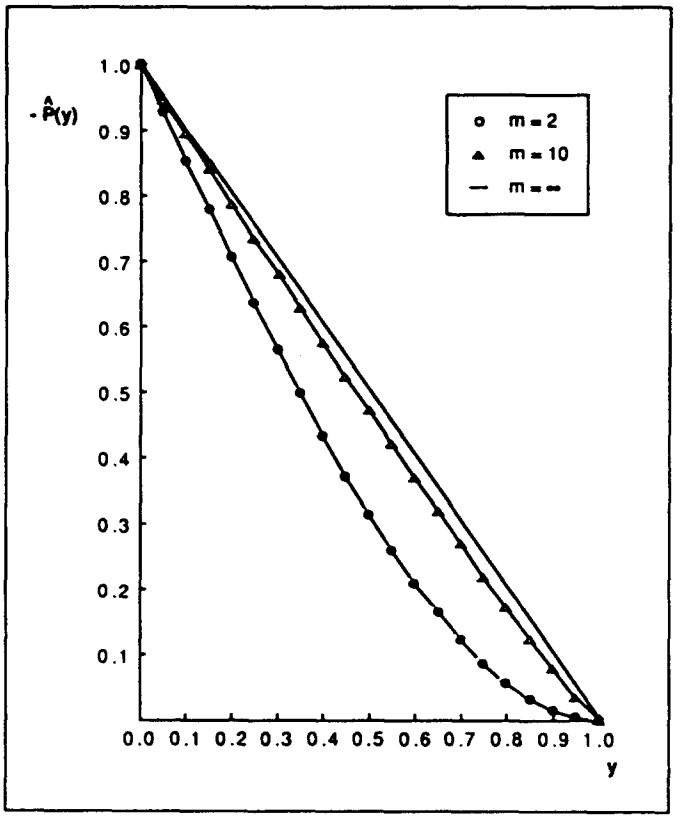

Fig. 4. Plot of nondimensional fiber force $\hat{P}(y)$ versus scaled distance y for $n = 1$ and several values of m. Later in the text $\hat{P}(y)$ is $H'(y\eta_{max})$.

$$\varepsilon_1(x,t) = -\frac{\phi}{2}\varepsilon\hat{\varepsilon}(y) = -\frac{\phi}{2}\varepsilon\hat{P}(y). \tag{42}$$

A plot of $\hat{P}(y)$ is shown in Fig. 4 for various values of m. The fiber displacements can be obtained by integrating the strains, i.e.

$$u_0(x,t) = \varepsilon^{(\alpha/\beta+1)}\left[1+\frac{\phi}{2}\right]^{\alpha/\beta} Q_3^{\alpha} t^{\alpha}\eta_{max}\left[\hat{u}(y)+\frac{\phi}{2}\hat{u}(0)\right], \tag{43}$$

and

$$u_1(x,t) = -\frac{\phi}{2}\varepsilon^{(\alpha/\beta+1)}\left[1+\frac{\phi}{2}\right]^{\alpha/\beta} Q_3^{\alpha} t^{\alpha}\eta_{max}[\hat{u}(y)-\hat{u}(0)], \tag{44}$$

where

$$\hat{u}(y) = \frac{2}{\sqrt{\pi}}\frac{\Gamma\{\beta+3/2\}}{\Gamma\{\beta+1\}}\int_y^1\left\{\int_z^1(1-\omega^2)^{\beta}\,d\omega\right\}dz. \tag{45}$$

Plots of $\hat{u}(y)$ are shown in Fig. 5 for several values of m.

Limiting behavior as $m \to \infty$. As m grows large, eqns (27), (30), (38) and (45) imply that $\eta_{max} \to 1$, $\hat{\tau}(y) \to 1$, $\hat{P}(y) \to (y-1)$ and $\hat{u}(y) \to (y-1)^2/2$. These limits are clearly evident on Figs 3–5. Also, it is evident from eqn (28) that as $m \to \infty$

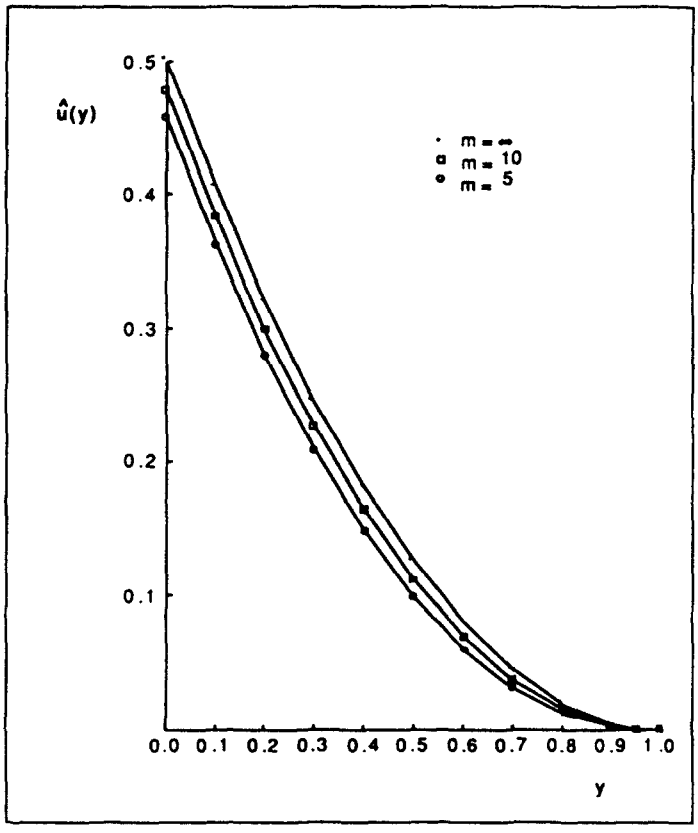

Fig. 5. Plot of nondimensional displacement $\hat{u}(y)$ versus scaled distance y for $n = 1$ and several values of m. Later in the text $\hat{u}(y)$ is $(\eta_{max})^{-1}H''(y\eta_{max})$.

$$x_{max} \to \frac{EA\varepsilon}{2D}, \text{ for all finite } t. \tag{46}$$

Note that $y = \eta/\eta_{max} = x/x_{max}$ and the fiber strains and forces tend towards

$$\varepsilon_0(x, t) \to \varepsilon(y-1), \tag{47}$$

$$\varepsilon_1(x, t) \to -\frac{\phi}{2}\varepsilon(y-1), \tag{48}$$

$$P_0(x, t) \to AE\varepsilon(y-1), \tag{49}$$

and

$$P_1(x, t) \to -\frac{AE\varepsilon}{2}(y-1), \tag{50}$$

which of course only apply for $0 \leqslant y \leqslant 1$, these quantities all being zero for $y > 1$. Also, as $m \to \infty$, the fiber displacements tend towards

$$u_0(x, t) \to \varepsilon^2\left[1+\frac{\phi}{2}\right]\left[\frac{(y-1)^2}{2}+\frac{\phi}{4}\right], \tag{51}$$

and

$$u_1(x,t) \to -\frac{\phi}{2}\varepsilon^2\left[1+\frac{\phi}{2}\right]\left[\frac{y^2}{2}-y\right]. \tag{52}$$

Lastly the shear stress approaches

$$\tau(x,t) \to 1. \tag{53}$$

Note that $\tau(x,t) \to 1$ is really a consequence of the assumed form of the matrix constitutive law. If we let $B = B'\tau_0^{-mn}$, thus yielding

$$\frac{\partial\gamma}{\partial t} = B'(\tau/\tau_0)^m, \tag{54}$$

for $n = 1$, then as $m \to \infty$, one anticipates that $\tau \to \tau_0$. Thus, behavior like that of a rigid, perfectly plastic matrix material would occur in the compression problem given large enough values of m.

Adaptation of results to tension version. The above results are easily adapted to the tension version of the problem using eqn (8). The shear stresses are unchanged as given by eqns (30), and η_{max} and x_{max} remain the same. The fiber strains are simply those for the compression problem with ε added, and the displacements are eqns (43) and (44) with εx added.

As for limiting results where $m \to \infty$, the matrix shear stress is unchanged and for the fiber strains simply add ε to the right-hand sides of eqns (47) and (48). For the displacements, simply add εx to eqns (51) and (52).

4. NUMERICAL SOLUTION OF THE CASE $n < 1$

Compression version. The closed form solution for the special case of $n = 1$ indicates the existence of x_{max} beyond which all displacements and stresses are identically zero. We look for a solution having the same feature for the general case of $n < 1$. It turns out that it is more convenient to define

$$U(x,t) = \frac{x\varepsilon(1+\phi/2)H(\eta)}{\eta}, \tag{55}$$

where H is related to g of eqn (16) by

$$H(\eta) = \eta g(\eta), \tag{56}$$

and η is still defined by eqn (17).

Following the same procedure as for $n = 1$, the governing equation for H is found to be [see Mason (1990)]:

$$H'' = H^{(1-n)/mn}\left[\frac{\alpha}{n}[H-\eta H']\right]^{1/m}, \tag{57}$$

which must be supplemented by the boundary conditions:

$$\begin{aligned} H(\eta = \eta_{max}) &= 0, \\ H'(\eta = \eta_{max}) &= 0, \\ H'(\eta = 0) &= -1. \end{aligned} \tag{58}$$

As in the case of $n = 1$, η_{max} is an unknown which is determined by the initial condition. η_{max} can be considered as an eigenvalue which is needed to satisfy the three conditions imposed by eqn (58). The existence of η_{max} implies that sufficiently far from the point of loading on the end of the center fiber, all fibers experience equal displacements so that their relative displacements and strains are identically zero. For the special case $\phi = 0$, all fiber displacements are identically zero at η_{max}.

Stresses, strains and displacements. From eqns (13) and (55), the shear stresses in the matrix are

$$\tau(x,t) = \frac{EA}{(2+\phi)D}\frac{\varepsilon(1+\phi/2)\eta}{x}H''(\eta)$$

$$= \frac{EA}{2D}\frac{\varepsilon\eta}{x}H''(\eta), \quad x < x_{max}, \tag{59}$$

independent of ϕ, where x_{max} is the length of the loaded or perturbed zone on the fibers, which by eqn (17) can be defined in terms of η_{max} as

$$x_{max} = \eta_{max}\varepsilon^{\alpha\beta}(1+\phi/2)^{\alpha\beta}Q_3^3t^2. \tag{60}$$

Note that for all $x > x_{max}$, all stress and strain quantities are identically zero. For the fiber strains, $\varepsilon_0(x,t) = u_{0,x}$ and $\varepsilon_1(x,t) = u_{1,x}$ we see from eqns (11) and (16) that

$$u_{0,x} = \varepsilon(1+\phi/2)H'(\eta) + u_{1,x}. \tag{61}$$

The fiber strains are also related by the overall equilibrium of the composite. For the compression version, there is no force applied at $x = \pm\infty$. Thus equilibrium requires that for all $x \geq 0$ and all $t > 0$,

$$EAu_{0,x} + 2\left[\frac{EA}{\phi}\right]u_{1,x} = 0. \tag{62}$$

Solving eqns (61) and (62) for $u_{0,x}$ and $u_{1,x}$ yields the strains

$$\varepsilon_0(x,t) = u_{0,x} = \varepsilon H'(\eta) \tag{63}$$

and

$$\varepsilon_0(x,t) = u_{1,x} = -\frac{\phi}{2}\varepsilon H'(\eta). \tag{64}$$

The displacements in Fiber 1 are obtained by integrating eqn (64) with respect to x, or equivalently, with respect to η with t held fixed. This yields

$$u_1(x,t) = \int_0^x \left\{-\frac{\phi}{2}\varepsilon H'(\eta)\right\}\mathrm{d}\tilde{x}$$

$$= \int_0^\eta \left\{-\frac{\phi}{2}\varepsilon H'(z)\right\}[\varepsilon^{\alpha\beta}(1+\phi/2)^{\alpha\beta}Q_3^3t^2]\,\mathrm{d}z$$

$$= \left\{-\frac{\phi}{2}\varepsilon^{(\alpha\beta+1)}(1+\phi/2)^{\alpha\beta}Q_3^3t^2\right\}\{H(\eta) - H(0)\}. \tag{65}$$

Similarly, the displacement in Fiber 0 is found to be

$$u_0(x,t) = \left\{\varepsilon x(1+\phi/2)\frac{H(\eta)}{\eta} - \frac{\phi}{2}\varepsilon^{(n\beta-1)}(1+\phi/2)^{n\beta}Q_3^n t^n\{H(\eta)-H(0)\}\right\}$$

$$= \varepsilon^{(n\beta-1)}(1+\phi/2)^{n\beta}Q_3^n t^n\{H(\eta)+(\phi/2)H(0)\}. \tag{66}$$

Note that when the outside fibers are rigid ($\phi = 0$) the displacement $u_1(x,t)$ of eqn (65) reduces to zero, and the displacement of the center fiber reduces to

$$u_0(x,t) = \varepsilon^{(n\beta+1)}Q_3^n t^n H(\eta). \tag{67}$$

The fiber forces are given by $P_0(x,t) = EAu_{0,x}$ and $P_1(x,t) = E_1Au_{1,x}$ and are found to be

$$P_0(x,t) = EA\varepsilon H'(\eta), \tag{68}$$

and

$$P_1(x,t) = -\frac{\phi}{2}\left[\frac{EA}{\phi}\right]\varepsilon H'(\eta)$$

$$= -\frac{EA}{2}\varepsilon H'(\eta). \tag{69}$$

Tension version. The solution to the problem of three fibers in tension at strain ε and with the middle fiber broken at $t = 0$ can be found using eqn (8). The shear stresses in the matrix involve relative fiber displacements, and thus, are unaffected. The length of the zone affected by unloading is still given by eqn (60). The fiber strains, fiber forces and fiber displacements are found to be

$$\tilde{\varepsilon}_0(x,t) = \varepsilon[1+H'(\eta)], \tag{70}$$

$$\tilde{\varepsilon}_1(x,t) = \varepsilon\left[1-\frac{\phi}{2}H'(\eta)\right], \tag{71}$$

$$\tilde{P}_0(x,t) = AE\varepsilon[1+H'(\eta)], \tag{72}$$

$$\tilde{P}_1(x,t) = \frac{AE\varepsilon}{\phi}\left[1-\frac{\phi}{2}H'(\eta)\right], \tag{73}$$

$$v_1(x,t) = \varepsilon^{(n/\beta+1)}\left[1+\frac{\phi}{2}\right]^{n/\beta}Q_3^n t^n\left\{\eta-\frac{\phi}{2}[H(\eta)-H(0)]\right\}, \tag{74}$$

$$v_0(x,t) = \varepsilon^{(n/\beta+1)}\left[1+\frac{\phi}{2}\right]^{n/\beta}Q_3^n t^n\left\{\left[1+\frac{\phi}{2}\right]H(\eta)-\eta-\frac{\phi}{2}H(0)\right\}, \tag{75}$$

respectively.

Numerical solution. Except for the case of $n = 1$, numerical solution of eqns (57) and (58) must be pursued as follows. Let

$$\mu = m \cdot n, \tag{76}$$

then eqn (57) can be rewritten as

$$H'' = H^{(1-n)\mu}\left[\frac{\chi}{n}(H-\eta H')\right]^{n\mu}, \quad 0 \leqslant \eta \leqslant \eta_{\max}. \tag{77}$$

Equation (77) is solved numerically to determine H and $\eta_{\max}(\mu, n)$, where the notation (μ, n) indicates the value $\eta_{\max}$ obtained for each pair of material parameters. There are three difficulties in the numerical calculations. First, a straightforward integration from the left end of the interval of interest is precluded, since the value of $H_0(\mu, n) \equiv H(\eta = 0)$ is unknown. Second, even though $H(\eta_{\max}) = 0$ and $H'(\eta_{\max}) = 0$, the value of $\eta_{\max}$ itself, is unknown, and consequently the extent of the region over which the solution is nonzero is unknown. Third, the values of all of the derivatives of $H(\eta)$ can be shown to be zero when η reaches $\eta_{\max}$. Consequently, $\eta_{\max}$ is a particularly undesirable point to begin an attempt at a numerical solution. Since $H'(\eta = 0) = -1$, the slope of $H(\eta = 0)$ is fixed for all values of μ and n, and a general computational approach is developed as follows. Choose a pair of μ and n values, then use the shooting method to generate a numerical solution for $H(\eta)$. Basically, a positive candidate value of H_0 is chosen, and eqn (77) is integrated forward from $\eta = 0$. This H_0 is checked by determining whether the boundary conditions $H(\eta_{\max}) = 0$ and $H'(\eta_{\max}) = 0$ are simultaneously met at some value of η. Iteration on H_0 continues until the boundary conditions are met to some desired degree of accuracy, and that value is denoted $H_0(\mu, n)$. Iteration for each pair of μ and n results in values for $H_0(\mu, n)$, $\eta_{\max}(\mu, n)$, and profiles of $H(\eta)$ and its derivatives.

Figure 6 shows numerical results for $H_0(\mu, n)$ plotted versus n for fixed values of μ. As μ becomes large, H_0 appears to tend towards 0.5 for all $0 \leqslant n \leqslant 1$. Also, at a fixed value of μ, as n increases, so does $H_0(\mu, n)$. This observation was useful in speeding up the $H_0(\mu, n)$ search procedure, as it produced better initial guesses for the $H_0(\mu, n)$ values, once $H_0(\mu, 0)$ and $H_0(\mu, 1)$ had been determined. Figure 7 shows numerical results for $\eta_{\max}(\mu, n)$ as a function of n using a log scale for the vertical axis. Note that the values for $\eta_{\max}(\mu, n)$ tend toward 1, regardless of n, as μ becomes large.

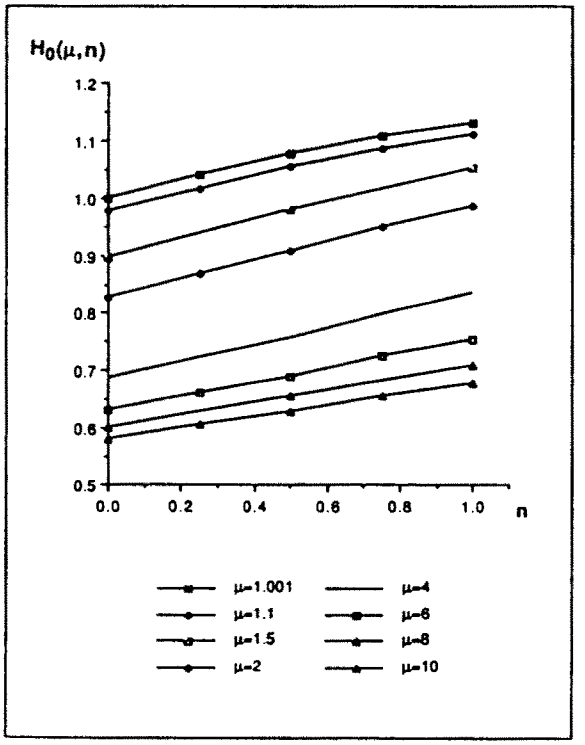

Fig. 6. Plot of $H_0(\mu, n) \equiv H(\eta = 0)$ versus n, showing the lines for values of μ between 1.001 and 10. $H_0(\mu, n)$ is a key factor in determining the displacements at the fiber break.

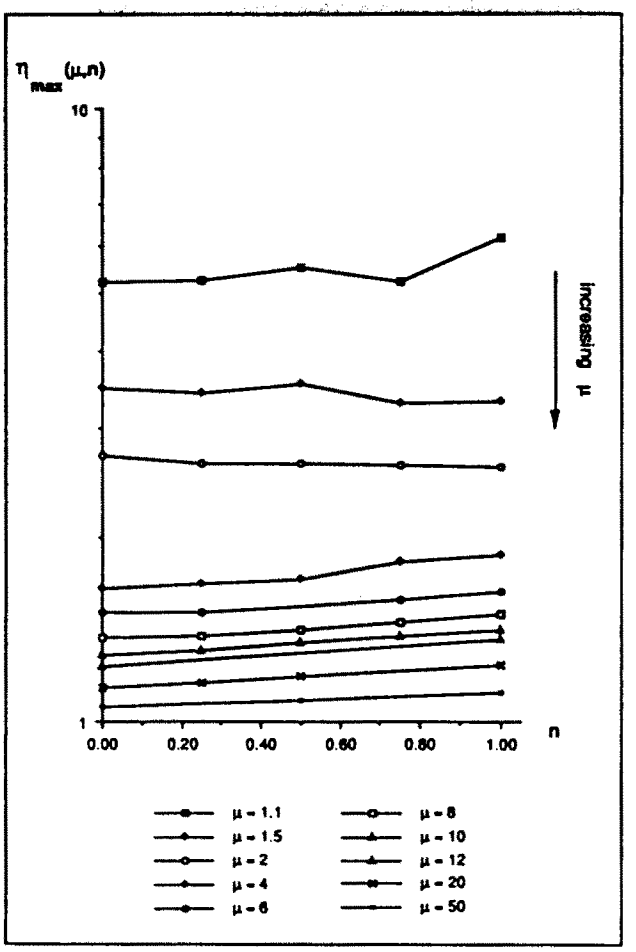

Fig. 7. Plots of perturbed distance factor η_{max} versus n for values of μ between 1.1 and 50. Note that η_{max} approaches 1 as μ increases for all n.

Some insight into the behavior of the numerical solutions for $H(\eta)$ is useful in evaluating Fig. 7. For relatively large values of μ, $\eta_{max}(\mu, n)$ is small, and the solutions for $H(\eta)$ look as though they will cross through the zero value that they are supposed to reach tangentially at η_{max}. Seemingly at the last instant, they curve sharply and "land" smoothly. The range of η values over which the solutions for $H(\eta)$ are near zero is quite small, and it is easy to distinguish the actual "landing point", or η_{max}. However, for small values of μ, the values of $\eta_{max}(\mu, n)$ are much larger and the approach of H to zero is more gradual, so that the numerically obtained η_{max} is less accurate. As μ becomes larger, however, the values for $\eta_{max}(\mu, n)$ are nearly straight lines when plotted linearly versus n. As a check on the validity of the numerical iteration scheme, the calculated values of $\eta_{max}(\mu = m, n = 1)$ were compared with the values predicted for this by eqn (27) with excellent agreement.

Letting $y = \eta/\eta_{max}$, Fig. 8 shows a plot of $H(y\eta_{max})$ versus y for $n = 0.5$ and $\mu = 1.001$, 2, 4, 10 and ∞. The displacements are related to $H(y\eta_{max})$ by eqns (65) and (66). $H(0)$ and the appropriate value for η_{max} can be obtained from Figs 6 and 7. For $n = 1$ the corresponding results were given in Fig. 5, and a plot of $H(y\eta_{max})$ for $n = 0$ is very similar to that in Fig. 8.

Figure 9 shows a plot of $H'(y\eta_{max})$ versus y for $n = 0.5$ and $\mu = 1.001$, 2, 4, 10 and ∞. The nondimensional fiber forces,

$$\hat{P}(y) = \frac{P_0(x, t)}{AE\varepsilon} = H'(y\eta_{max}), \tag{78}$$

or the normalized strain,

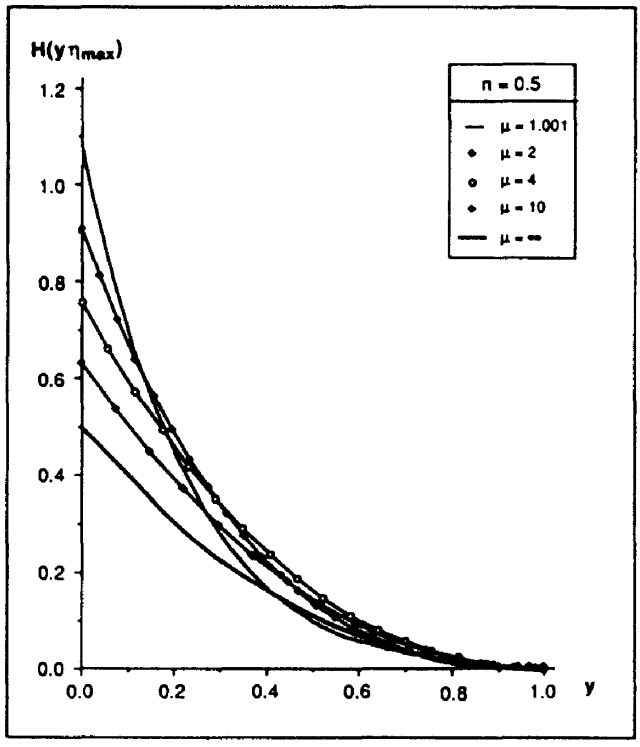

Fig. 8. Plots of $H(y\eta_{max})$ versus $y = \eta/\eta_{max}$ for $n = 0.5$ and $\mu = 1.001$, 2, 4, 10 and ∞. Note that $H(y\eta_{max}) = \hat{u}(y)\eta_{max}$ where $\hat{u}(y)$ is nondimensional displacement.

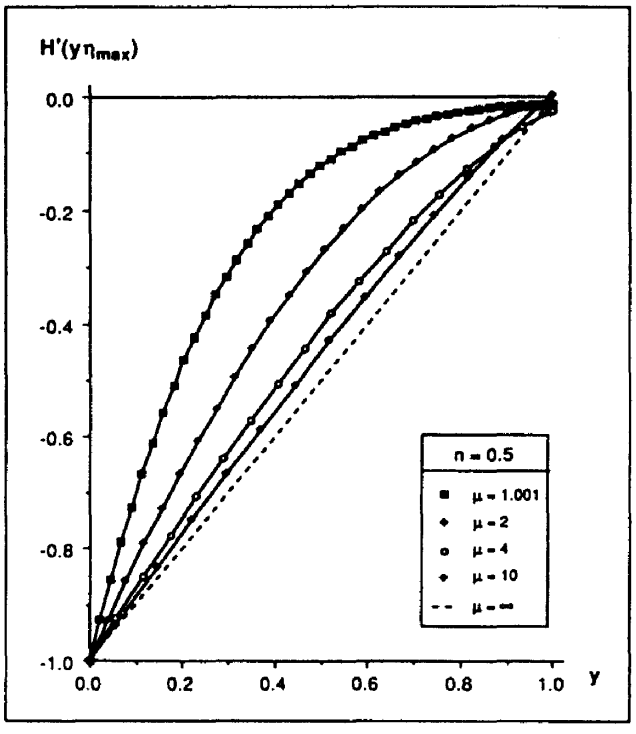

Fig. 9. Plot of nondimensional fiber force $\hat{P}(y) = H'(y\eta_{max})$ versus scaled distance y for $n = 0.5$ and $\mu = 1.001$, 2, 4, 10 and ∞.

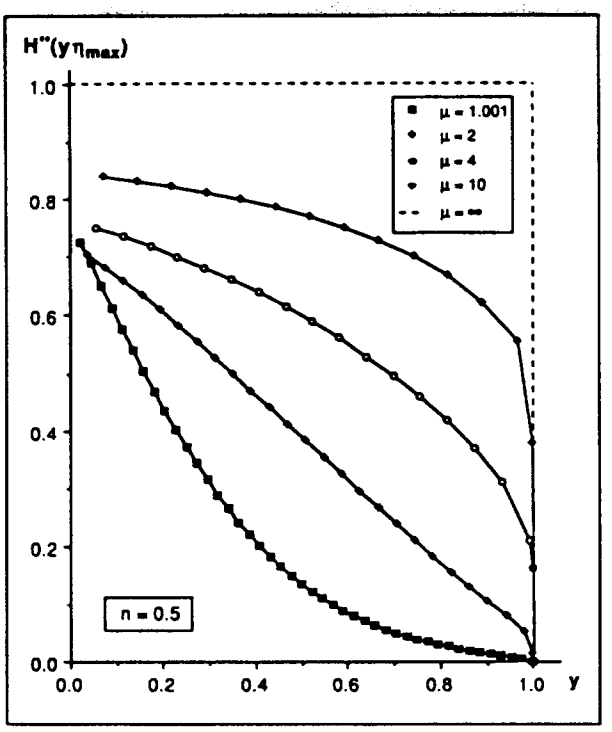

Fig. 10. Plot of $H''(y\eta_{max})$ versus scaled distance y for $n = 0.5$ and $\mu = 1.001, 2, 4, 10$ and ∞. Note that $H''(y\eta_{max}) = \hat{\tau}(y)/\eta_{max}$ where $\hat{\tau}(y)$ is nondimensional shear stress.

$$\hat{\varepsilon}(y) = \frac{\varepsilon_0(x,t)}{\varepsilon} = \hat{P}(y), \tag{79}$$

may be obtained directly from this figure using the appropriate value for η_{max} from Fig. 7. For $n = 1$ corresponding results were given in Fig. 4, and a plot of $H'(y\eta_{max})$ for $n = 0$ turns out to be very similar to that in Fig. 9.

Figure 10 shows a plot of $H''(y\eta_{max})$ versus y for $n = 0$ and $\mu = 1.001, 2, 4, 10$ and ∞. The shear stress may be obtained from these figures using eqn (59) and the appropriate values of η_{max} from Fig. 7. For $n = 1$ the corresponding results were given in Fig. 3, and a plot of $H''(y\eta_{max})$ for $n = 0$ turns out to be similar to that in Fig. 10.

5. EXTENSION TO FIVE FIBER COMPOSITE

The previous analysis is extended to a composite with five fibers as shown in Fig. 11. The description of the model is the same as that of Section 2, except that there are now five fibers dividing four equal bays of matrix. The fibers are denoted $-2, -1, 0, 1$ and 2, which will also appear as subscripts on associated quantities. The Young's modulus for Fiber 0 is $E_0 = E/\phi_0$, for Fibers -1 and 1 is E, and for Fibers -2 and 2 is $E_2 = E/\phi_2$, where $0 < \phi_0 \leqslant 1$ and $0 < \phi_2 \leqslant 1$. For the most part we concentrate on the case $\phi_2 = 1$.

Tension version. The five fibers are loaded at $x = \pm\infty$, by whatever forces are necessary to produce a uniform strain, ε. Thus $P_0 = AE\varepsilon/\phi_0$, $P_1 = P_{-1} = AE\varepsilon$ and $P_2 = P_{-2} = AE\varepsilon/\phi_2$. At $t = 0$, Fiber 0 is suddenly broken at $x = 0$. An unloaded zone develops at the end of the broken fiber and the intact fibers are overloaded along some time dependent length. Due to symmetry, the displacements, strains and forces in Fiber k will be identical to those in Fiber $-k$, for $k = 1, 2$. The shear stress transmitted by the matrix between Fibers k and $k-1$ is denoted $\tau_k(x,t)$, and clearly $\tau_k(x,t) = -\tau_{-k}(x,t)$. Due to symmetry, we restrict our attention to Fibers 0, 1 and 2 and matrix Bays 1 and 2.

Equation (4) holds for Fiber 0 but with E taken as E/ϕ_0 and τ taken as τ_1, and

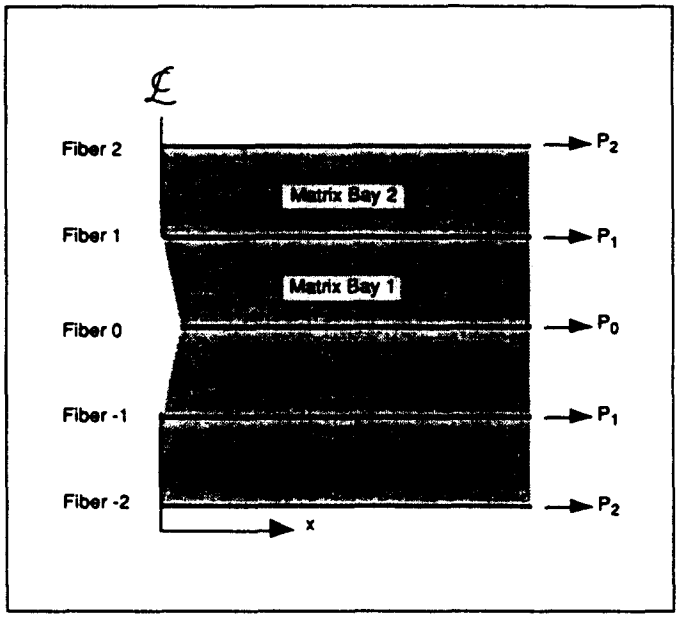

Fig. 11. Configuration for the tension version of the five-fiber problem with fiber stiffnesses $E_0 = E/\phi_0$, $E_1 = E$ and $E_2 = E/\phi_2$.

$$D[\tau_1(x,t)-\tau_2(x,t)] = -EA\frac{\partial^2 v_1(x,t)}{\partial x^2}, \tag{80}$$

applies for Fiber 1. Also, for Fiber 2

$$\tau_2(x,t) = \frac{EA}{\phi_2 D}\left[-\frac{\partial^2 v_2(x,t)}{\partial x^2}\right]. \tag{81}$$

For $i = 1, 2$ let $\gamma_i(x,t)$ be the matrix shear strain for Bay i so that

$$\frac{\partial \gamma_i(x,t)}{\partial t} = \frac{1}{d}\frac{\partial}{\partial t}[v_{(i-1)}(x,t)-v_i(x,t)], \tag{82}$$

for two adjacent fibers. Thus, using the constitutive law, eqn (1), we obtain

$$\frac{\partial}{\partial t}[v_0-v_1] = dB\left[\frac{EA}{2\phi_0 D}\right]^{mn}[v_{0,xx}]^m n\left[\int_0^t [v_{0,xx}]^m\,ds\right]^{n-1}, \tag{83}$$

for Bay 1, and for Bay 2 we obtain

$$\frac{\partial}{\partial t}[v_1-v_2] = dB\left[\frac{EA}{\phi_2 D}\right]^{mn}[-v_{2,xx}]^m n\left[\int_0^t [-v_{2,xx}]^m\,ds\right]^{n-1}, \tag{84}$$

where we have assumed that $v_{0,xx} \geqslant 0$ and $-v_{2,xx} \geqslant 0$ for all $x \geqslant 0$ and $t > 0$. Equations (83) and (84) are the coupled equations written in terms of the fiber displacements. The boundary and initial conditions are:

$$\left.\begin{aligned} v_k(x>0, t=0) &= \varepsilon x \\ v_{k,x}(x\to\infty, t\geqslant 0) &= \varepsilon \end{aligned}\right\} \quad \text{for} \quad k = 0, 1 \text{ and } 2.$$

$$v_i(x=0, t>0) = 0, \qquad \text{for} \quad i = 1 \text{ and } 2.$$

$$v_{0,x}(x=0,t>0)=0.$$

$$v_{1,x}(x=0,t>0)+\frac{1}{\phi_2}v_{2,x}(x=0,t>0)=\varepsilon\left[\frac{1}{2\phi_0}+1+\frac{1}{\phi_2}\right]. \tag{85}$$

The last equation here represents overall composite force equilibrium.

Compression version. In the compression version where no forces are applied at $x=\pm\infty$ and compressive forces are suddenly applied to broken fiber ends at $t=0$, the displacements $u_k(x,t)$ are·

$$u_k(x,t)=v_k(x,t)-\varepsilon x, \quad \text{for} \quad k=0, 1 \text{ and } 2. \tag{86}$$

We assume the fibers are initially unstrained and quiescent and Fiber 0 is already broken at $x=0$. Then at $x=0$ and $t=0$, a compressive force $P_0=AE\varepsilon/\phi_0$ is suddenly applied to Fiber 0, and a loaded zone develops. The governing equations for the compression problem are given by eqns (83) and (84) with u_k in place of v_k, and the initial and boundary conditions are:

$$\left.\begin{aligned}&u_k(x>0,t=0)=0\\&u_{k,x}(x\to\infty,t\geqslant 0)=0\end{aligned}\right\} \quad \text{for} \quad k=0, 1 \text{ and } 2.$$

$$u_i(x=0,t>0)=0, \qquad \text{for} \quad i=1 \text{ and } 2.$$

$$u_{0,x}(x=0,t>0)=-\varepsilon.$$

$$u_{1,x}(x=0,t>0)+\frac{1}{\phi_2}u_{2,x}(x=0,t>0)=\frac{\varepsilon}{2\phi_0}. \tag{87}$$

Self-similar transformation. As with three fibers, a self-similar form is assumed for the five-fiber problem. We define Q_5 by

$$Q_5=(dB)^{1/n}\left[\frac{EA}{D}\right]^m. \tag{88}$$

The similarity variable, η is defined in terms of Q_5 as

$$\eta=\frac{x}{\varepsilon^{\alpha/\beta}Q_5^{\alpha}t^{\alpha}}. \tag{89}$$

The solution for the fiber displacements is assumed to be of the form

$$u_k(x,t)=x\varepsilon\frac{h_k(\eta)}{\eta}, \tag{90}$$

for $k=0$, ± 1 and ± 2. We further assume that there exist solutions to the governing coupled equations subject to the existence of a finite value of η common to all fibers, called η_{max}, such that for all $\eta>\eta_{max}$, all displacements and their derivatives are identically zero. Following the manipulations in Sections 2 and 3, we derive the coupled governing equations for $h_k(h)$ as

$$h_0''=2\phi_0\left[\frac{\alpha}{n}\right]^{1/m}[h_0-h_1]^{(1-n)/mn}[(h_0-h_1)-\eta(h_0'-h_1')]^{1/m}, \tag{91}$$

and

$$-h_2'' = \phi_2\left[\frac{x}{n}\right]^{1/m}[h_1-h_2]^{(1-n)/mn}[(h_1-h_2)-\eta(h_1'-h_2')]^{1/m}. \tag{92}$$

From equilibrium of the composite we also have

$$h_1''(\eta) = -\left[\frac{1}{\phi_2}h_2''(\eta)+\frac{1}{2\phi_0}h_0''(\eta)\right]. \tag{93}$$

From these constructions, the boundary and initial conditions, eqns (87), become

$$\begin{aligned} h_0(\eta=\eta_{\max}) &= h_1(\eta=\eta_{\max}) = h_2(\eta=\eta_{\max}),\\ h_k'(\eta=\eta_{\max}) &= 0, \qquad k=0,1 \text{ and } 2,\\ h_k''(\eta=\eta_{\max}) &= 0, \qquad k=0,1 \text{ and } 2,\\ h_0'(\eta=0) &= -1, \quad k=0,1 \text{ and } 2,\\ h_1'(\eta=0)+h_2'(\eta=0)/\phi_2 &= 1/(2\phi_0). \end{aligned} \tag{94}$$

Matrix shear stresses. From eqns (4), (80) and (81) the matrix shear stresses can be written in terms of the functions $h_k(\eta)$ and their derivatives. For convenience in plotting, we let nondimensional shear stresses be defined as

$$\begin{aligned} \hat{\tau}_1(y) &= \frac{2\phi_0 D\eta_{\max}}{EA}\varepsilon^{(\alpha+\beta-1)}Q_5^2 t^2\tau_1(x,t)\\ &= \eta_{\max}h_0''(y\eta_{\max}) \end{aligned} \tag{95}$$

for Bay 1 and

$$\begin{aligned} \hat{\tau}_2(y) &= \frac{\phi_2 D\eta_{\max}}{EA}\varepsilon^{(\alpha+\beta-1)}Q_5^2 t^2\tau_2(x,t)\\ &= -\eta_{\max}h_2''(y\eta_{\max}) \end{aligned} \tag{96}$$

for Bay 2. The shear stresses are readily obtained from plots of $h_0''(y\eta_{\max})$ and $h_2''(y\eta_{\max})$ as considered shortly.

Fiber displacements, forces and strains. From eqn (90) the fiber displacements may be formulated in nondimensional terms as

$$\begin{aligned} \hat{u}_k(y) &= \frac{u_k(x,t)}{\eta_{\max}\varepsilon^{(1+\alpha+\beta)}Q_5^2 t^2}\\ &= \frac{1}{\eta_{\max}}h_k(y\eta_{\max}), \end{aligned} \tag{97}$$

for $k = 0$, 1 and 2. The individual fiber forces and strains may be written in nondimensional terms, using eqn (90), as

$$\begin{aligned} \hat{P}_0(y) &= \frac{\phi_0}{EA\varepsilon}P_0(x,t) = h_0'(y\eta_{\max}),\\ \hat{P}_1(y) &= \frac{1}{EA\varepsilon}P_1(x,t) = h_1'(y\eta_{\max}),\\ \hat{P}_2(y) &= \frac{\phi_2}{EA\varepsilon}P_2(x,t) = h_2'(y\eta_{\max}), \end{aligned} \tag{98}$$

$$\hat{\varepsilon}_i(y) = \frac{\varepsilon_i(x,t)}{\varepsilon} = \hat{P}_i(y) = h_i'(y\eta_{\max}), \quad \text{for} \quad i = 1, 2 \text{ and } 3. \tag{99}$$

Plots of $h_0'(y\eta_{\max})$, $h_1'(y\eta_{\max})$ and $h_2'(y\eta_{\max})$ are considered shortly.

Plastic-like behavior for large m. It is interesting to examine the behavior of the compression version as $m \to \infty$. As m increases, the matrix material approaches the behavior of a rigid, perfectly plastic material. A solution to the governing equations (91)–(94), is fairly straightforward using polynomial forms for $h_k(\eta)$ and recognizing that $h_0''(\eta) = 2\phi_0$ and $h_2''(\eta) = C\phi_2$ for some negative constant C [see Mason (1990)]. It is found that $\eta_{\max} = 1/(2\phi_0)$ and

$$h_0(\eta) = \phi_0\eta^2 - \eta + \left[\frac{\phi_2}{8\phi_0^2(\phi_2+1)} + \frac{1}{4\phi_0}\right],$$

$$h_1(\eta) = h_2(\eta) = \frac{\phi_2}{2(\phi_2+1)}\left[-\eta^2 + \frac{1}{\phi_0}\eta\right], \tag{100}$$

for $0 \leqslant \eta \leqslant \eta_{\max}$. The nondimensional fiber forces and strains of eqns (98) and (99) are linear in η according to

$$h_0'(\eta) = 2\phi_0\eta - 1,$$

$$h_1'(\eta) = h_2'(\eta) = \frac{\phi_2}{\phi_2+1}\left[\frac{1}{2\phi_0} - \eta\right]. \tag{101}$$

Thus for the case of rigid perfectly plastic matrix ($m \to \infty$), the displacements and strains in Fibers 1 and 2 are identical, regardless of their relative stiffnesses. When $\phi_0 = \phi_2 = 1$, all five fibers have equal stiffness, E. From eqns (95) (101) we obtain the following results: The nondimensional matrix shear stresses are

$$\hat{\tau}_1(y) = 1, \tag{102}$$

$$\hat{\tau}_2(y) = \tfrac{1}{4}, \tag{103}$$

where $\eta = y\eta_{\max}$ or $x = yx_{\max}$. The nondimensional fiber forces and strains are

$$\hat{P}_0(y) = y - 1, \tag{104}$$

$$\hat{P}_1(y) = \hat{P}_2(y) = \tfrac{1}{4}(1-y), \tag{105}$$

and the nondimensional fiber displacements are

$$\hat{u}_0(y) = \tfrac{1}{2}y^2 - \tfrac{1}{4}y + \tfrac{5}{8}, \tag{106}$$

$$\hat{u}_1(y) = \hat{u}_2(y) = -\tfrac{1}{8}y^2 + \tfrac{1}{4}y. \tag{107}$$

Numerical results for $\phi_0 = \phi_2 = 1$. A shooting method algorithm has been developed to solve the governing equations (91)–(94) for the case $\phi_0 = \phi_2 = 1$ (equal fiber stiffness). As in Section 4, the results are given in terms of $\mu = m \cdot n$ and n. The region, $0 \leqslant \eta \leqslant \eta_{\max}$, over which the functions $h_k(\eta)$, $k = 0, 1$ and 2, are defined and their derivatives are nonzero, is of undetermined length. At the end of the interval $\eta_{\max}$, all derivatives of the $h_k(\eta)$ are identically zero, and $h_0(\eta_{\max}) = h_1(\eta_{\max}) = h_2(\eta_{\max})$. In this problem, iteration takes place on values for two boundary conditions, $h_0(\eta = 0)$ and $h_1'(\eta = 0)$, which must be determined for each set of material parameters μ and n. For each iteration, the successive choices of

$h_0(\eta = 0)$ and $h_1'(\eta = 0)$ are tested for "goodness" by determining whether the conditions for η_{max} are simultaneously satisfied for all functions $h_k(\eta)$ at some point η. That value of η is denoted $\eta_{max}(\mu, n)$, and the corresponding values of the Fiber 0 displacement and the Fiber 1 strain at $\eta = 0$ are denoted $h_0^*(\mu, n)$ and $h_1'(\mu, n)$, respectively.

The numerical iteration procedure was carried out for values of μ between 1.25 and 6, and values of n between 0.01 and 0.99. Although the solutions for the $h_k(\eta)$ are quite smooth functions, it was necessary to determine the initial conditions to within 10^{-6} in order to satisfy the boundary conditions at η_{max}. Even so, the accurate determination of η_{max} was difficult for larger values of μ.

Figures 12 and 13 are plots of the numerical results for $h_0^*(\mu, n)$ and $h_1'(\mu, n)$ respectively, which are useful for determining the end displacements for Fiber 0 and neighboring strain induced in Fiber 1. From eqn (100), as $m \to \infty$ and $\mu \to \infty$ the values for $h_0^*(\mu, n)$ and $h_1'(\mu, n)$ approach 5/16 and 1/4 respectively since $\phi_0 = \phi_2 = 1$. The numerical results plotted in these figures approach that limit. Figure 13 indicates that the increase in strain on the flanking fibers depends primarily on the value of $\mu = mn$ rather than on n. For μ near one the neighboring fiber bears most of the overload but this diminishes to equal sharing among all four flanking fibers as μ increases.

Figure 14 is a plot of η_{max} versus n. As $m \to \infty$ and $\mu \to \infty$, the limiting value of η_{max} was determined earlier to be 1/2. Note that fairly large values of μ are needed to approach this limit.

Figure 15 shows plots of the functions $h_0(y\eta_{max})$, $h_1(y\eta_{max})$ and $h_2(y\eta_{max})$ versus y for $\mu = 4$ and $n = 0.7$. The nondimensional fiber displacements, as defined in eqn (97), may be obtained from these plots by scaling with the value of η_{max} from Fig. 14.

Figure 16 shows plots of $h_0'(y\eta_{max})$, $h_1'(y\eta_{max})$ and $h_2'(y\eta_{max})$ versus y for $\mu = 4$ and $n = 0.7$. These curves are the nondimensional fiber forces and strains as defined in eqns (98) and (99). Note that the strain in Fiber 2 is actually greater than the strain in Fiber 1 for larger y, so that the outside fibers carry more of the excess load from the broken fiber, until the end of the overload zone is reached.

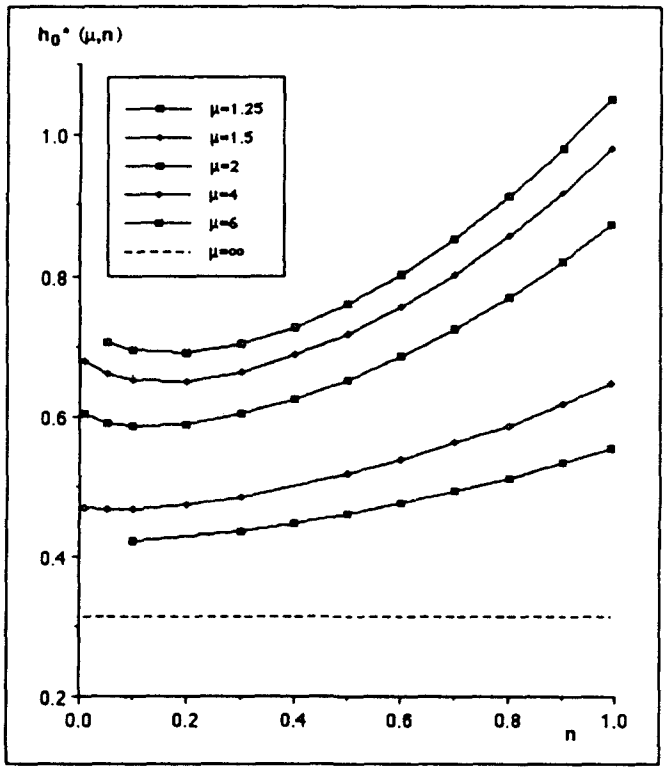

Fig. 12. Plot of numerical results for Fiber 0 displacement factor $h_0^*(\mu, n)$ versus n for various μ. The limiting case of $\mu \to \infty$ is also shown.

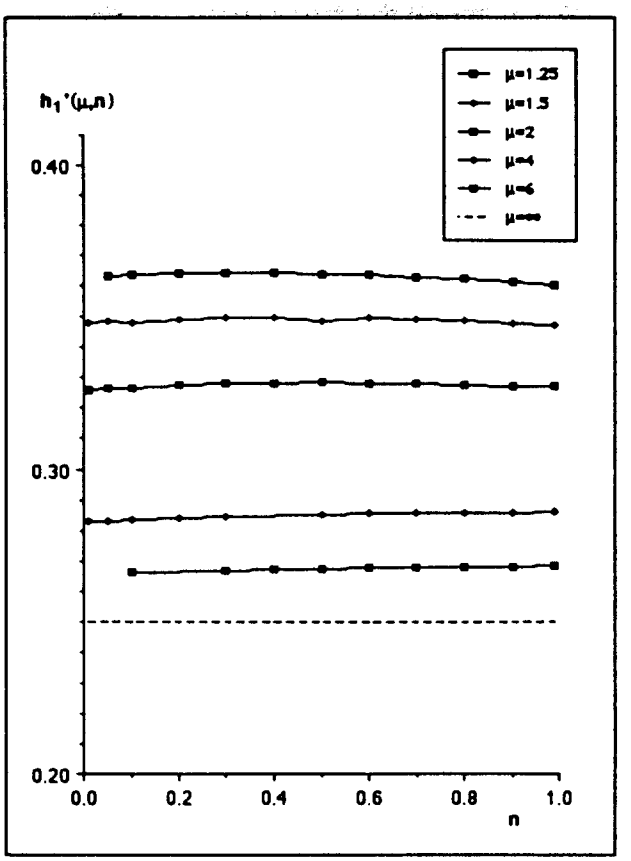

Fig. 13. Plot of numerical results for Fiber 1 strain factor $h_1'(\mu, n)$ versus n for various μ. The limiting case of $\mu \to \infty$ is also shown.

Figure 17 shows plots of the functions $h_0''(y\eta_{\max})$, $h_1''(y\eta_{\max})$ and $h_2''(y\eta_{\max})$ versus y for $\mu = 4$ and $n = 0.7$. The nondimensional shear stresses as given in eqn (95) may be obtain from these curves by scaling with the appropriate value of $\eta_{\max}$ from Fig. 14.

Recovering the tension problem results. It is now relatively straightforward to reconstruct the results of the tension version from those of the compression version. As was the case earlier, the shear stresses are identical for both problems. For the displacements we have

$$\begin{aligned} v_k(x,t) &= \frac{x\varepsilon}{\eta} h_k(\eta) + x\varepsilon \\ &= \varepsilon^{(1+\alpha/\beta)} Q_3^{\alpha} t^{\alpha} [h_k(\eta) + \eta], \end{aligned} \tag{108}$$

and for the fiber strains $\varepsilon_k(x,t)$ we have

$$\begin{aligned} \varepsilon_k(x,t) &= \frac{\partial v_k(x,t)}{\partial x} = \frac{\partial u_k(x,t)}{\partial x} + \varepsilon \\ &= \varepsilon[h_k'(\eta) + 1]. \end{aligned} \tag{109}$$

Thus the fiber forces are

$$\begin{aligned} \tilde{P}_0(x,t) &= \frac{EA\varepsilon}{\phi_0}[h_0'(\eta) + 1], \\ \tilde{P}_1(x,t) &= EA\varepsilon[h_1'(\eta) + 1], \end{aligned} \tag{110}$$

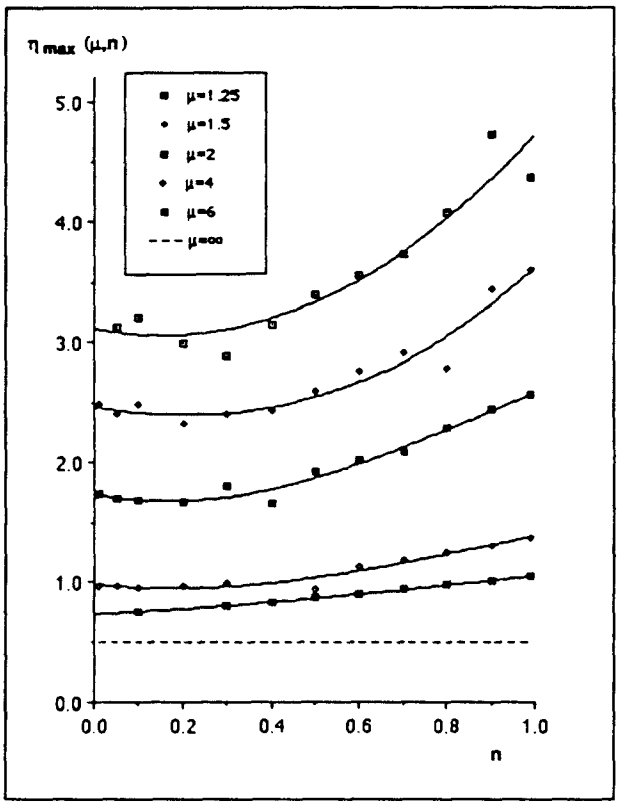

Fig. 14. Plot of numerical results for perturbed distance factor $\eta_{max}(\mu, n)$ versus n for various μ. Lines through the data are cubic fits. The limit for $\mu \to \infty$ is also shown.

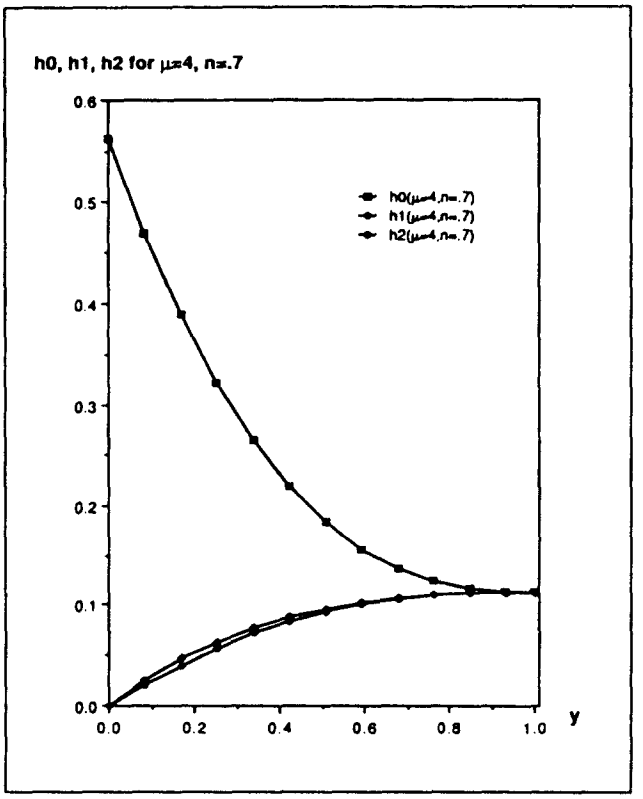

Fig. 15. Plots of numerical results for $h_0(y\eta_{max})$, $h_1(y\eta_{max})$ and $h_2(y\eta_{max})$, for $\mu = 4$, $n = 0.7$. When divided by η_{max} these are the nondimensional fiber displacements and the curves are typical of the general curve shapes for different μ and n pairs.

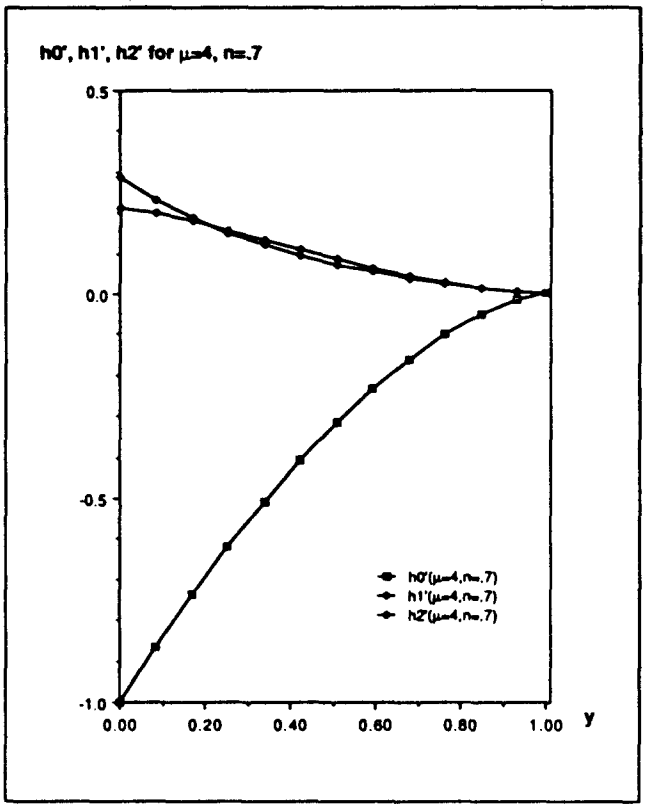

Fig. 16. Plots of numerical results for $h_0'(y\eta_{max})$, $h_1'(y\eta_{max})$ and $h_2'(y\eta_{max})$, for $\mu = 4$ and $n = 0.7$. These are nondimensional fiber forces and the curves are typical of the general curve shapes for different μ and n pairs.

$$\tilde{P}_2(x,t) = \frac{EA\varepsilon}{\phi_2}[h_2'(\eta)+1]. \tag{111}$$

These quantities are all easily visualized from Figs 15–17.

6. CONCLUSIONS

The creep behavior of the matrix in shear has the following important implications on the time behavior of the stress fields near a fiber break.

(1) The overload region on the intact fibers grows in time in a self-similar way and typically has a finite extent beyond which there is no disturbance. The shape of this overload profile is roughly triangular.

(2) The effective load transfer length grows in time t as $t^{n/(mn+1)}$, where n and m are respectively the exponents for time and stress level in the matrix constitutive law.

(3) The effective load transfer length grows with the composite strain level ε in proportion to $\varepsilon^{(mn-1)/(mn+1)}$.

(4) The displacement of the broken fiber end grows as $\varepsilon^{2mn/(mn+1)}$ and $t^{n/(mn+1)}$.

(5) The fraction of the overload shifted from the broken fiber to adjacent and subadjacent fibers, respectively, depends on the value of m and n and is not fixed as in the case of linear viscoelasticity.

An indentation experiment may be devised whereby a strain ε is imposed on the end of a broken fiber flanked by two fibers of much larger stiffness AE. The theory here may be adapted, and by measuring the time growth of the end displacement and its dependence on ε, the exponents m and n may be estimated.

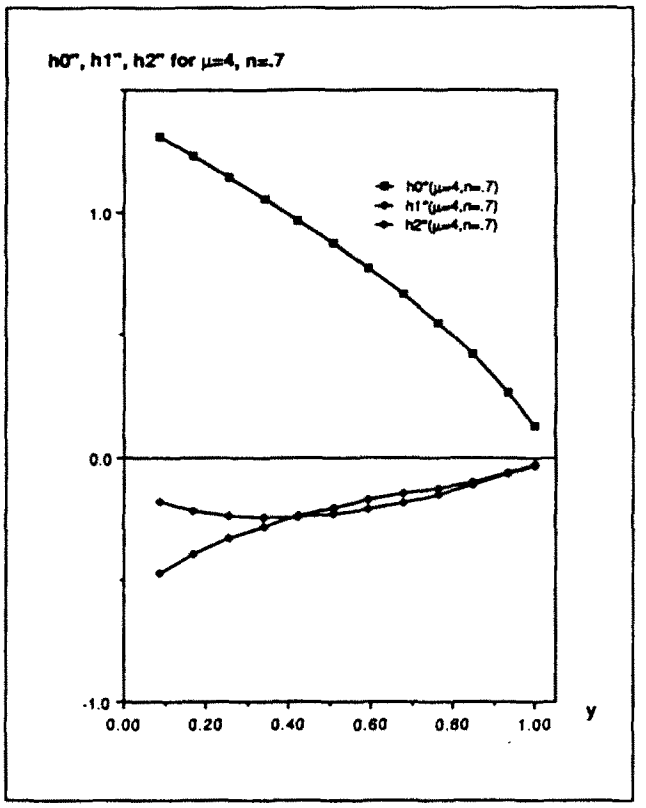

Fig. 17. Plots of numerical results for $h_0''(y\eta_{max})$, $h_1''(y\eta_{max})$ and $h_2''(y\eta_{max})$, for $\mu = 4$ and $n = 0.7$. When multiplied by η_{max} the first and last are the nondimensional shear stresses in the Matrix Bays 1 and 2 respectively, and the curves are typical of the general curve shapes for different μ and n pairs.

Acknowledgements—This work was supported by the Cornell Materials Science Center, which is funded by the National Science Foundation (DMR-MRL program).

REFERENCES

Glad, M. D. (1986). Microdeformation and network structures in epoxies. Ph.D. Thesis, Cornell University.

Goree, J. G. and Gross, R. S. (1979). Analysis of a unidirectional composite containing broken fibers and matrix damage. *Engng Fract. Mech.* **13**, 563–578.

Goree, J. G. and Gross, R. S. (1980). Stresses in a three-dimensional unidirectional composite containing broken fibers. *Engng Fract. Mech.* **13**, 395–405.

Gulino, R., Schwartz, P. and Phoenix, S. L. (1991). Experiments on shear deformation, debonding and local load transfer in a model graphite/glass/epoxy microcomposite. *J. Materials Science* **26**, 6655–6672.

Hedgepeth, J. M. (1961). Stress concentrations in filamentary structures. NASA TN D-882, Langley Research Center.

Hedgepeth, J. M. and Van Dyke, P. (1967). Local stress concentrations in imperfect filamentary composite materials. *J. Composite Mater.* **1**, 294–309.

Lagoudas, D. C., Hui, C.-Y. and Phoenix, S. L. (1989). Time evolution of overstress profiles near broken fibers in a composite with a viscoelastic matrix. *Int. J. Solids Structures* **25**, 45–66.

Lifshitz, J. M. and Rotem, A. (1970). Time-dependent longitudinal strength of unidirectional fibrous composites. *Fibre Sci. Technol.* **3**, 1–20.

Mason, D. D. (1990). Time dependence of the displacement fields around fiber breaks in a composite with a power-law creeping matrix. Ph.D. Thesis, Cornell University.

Otani, H., Phoenix, S. L. and Petrina, P. (1991). Matrix effects on lifetime statistics for carbon fiber/epoxy microcomposites in creep rupture. *J. Materials Science* **26**, 1955–1970.

Phoenix, S. L., Schwartz, P. and Robinson IV, H. H. (1988). Statistics for the strength and lifetime in creep-rupture of model carbon/epoxy composites. *Composites Sci. Technol.* **32**, 81–120.

Phoenix, S. L. and Tierney, L.-J. (1983). A statistical model for the time dependent failure of unidirectional composite materials under local elastic load-sharing among fibers. *Engng Fract. Mech.* **18**, 193–215.